



HAL
open science

Analysis of process parameters influence on syngas yields and biomass gasification rates in a continuous particle-fed solar-irradiated gasifier

Srirat Chuayboon, Stéphane Abanades, Sylvain Rodat

► **To cite this version:**

Srirat Chuayboon, Stéphane Abanades, Sylvain Rodat. Analysis of process parameters influence on syngas yields and biomass gasification rates in a continuous particle-fed solar-irradiated gasifier. AIP Conference Proceedings, 2020, pp.170005. 10.1063/5.0028586 . hal-03077636

HAL Id: hal-03077636

<https://hal.science/hal-03077636>

Submitted on 16 Dec 2020

HAL is a multi-disciplinary open access archive for the deposit and dissemination of scientific research documents, whether they are published or not. The documents may come from teaching and research institutions in France or abroad, or from public or private research centers.

L'archive ouverte pluridisciplinaire **HAL**, est destinée au dépôt et à la diffusion de documents scientifiques de niveau recherche, publiés ou non, émanant des établissements d'enseignement et de recherche français ou étrangers, des laboratoires publics ou privés.

Analysis of process parameters influence on syngas yields and biomass gasification rates in a continuous particle-fed solar-irradiated gasifier

Cite as: AIP Conference Proceedings **2303**, 170005 (2020); <https://doi.org/10.1063/5.0028586>
 Published Online: 11 December 2020

Srirat Chuayboon, Stéphane Abanades, and Sylvain Rodat



View Online



Export Citation

ARTICLES YOU MAY BE INTERESTED IN

[Solar redox cycling of ceria in a monolithic reactor for two-step H₂O/CO₂ splitting: Isothermal methane-induced reduction versus temperature-swing cycle](#)

AIP Conference Proceedings **2303**, 170009 (2020); <https://doi.org/10.1063/5.0028582>



Your Qubits. Measured.

Meet the next generation of quantum analyzers

- Readout for up to 64 qubits
- Operation at up to 8.5 GHz, mixer-calibration-free
- Signal optimization with minimal latency

Find out more



Analysis of Process Parameters Influence on Syngas Yields and Biomass Gasification Rates in a Continuous Particle-Fed Solar-Irradiated Gasifier

Srirat Chuayboon^{1, 2}, Stéphane Abanades^{1, a)}, and Sylvain Rodat¹

¹ Processes, Materials and Solar Energy Laboratory, PROMES-CNRS, 7 Rue du Four Solaire, 66120 Font-Romeu, France

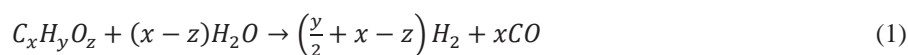
² Department of Mechanical Engineering, King Mongkut's Institute of Technology Ladkrabang, Prince of Chumphon Campus, Chumphon 86160, Thailand

^{a)} Corresponding author: stephane.abanades@promes.cnrs.fr

Abstract. Steam gasification of biomass was experimentally investigated with different lignocellulosic biomass feedstocks in a 1.5 kW_{th} continuous particle-fed solar-irradiated gasifier at high temperatures (1100-1300 °C) utilizing highly concentrated sunlight as process heat source, demonstrating the conversion of intermittent solar energy and biomass into synthesis gas without CO₂ emissions. Forty-nine on-sun experiments were performed in order to study the effect of process parameters (biomass feeding rate, temperature, biomass composition) on syngas production yield, biomass gasification rate (carbon conversion rate), and reactor performance. As a result, syngas yield, composition (quality), biomass gasification rate, and reactor performance increase significantly with both the biomass feeding rate and temperature because both biomass consumption rates and reaction kinetics are enhanced. However, the performance outputs are reduced when biomass feeding rate exceeds its optimal feeding point. The reactor temperature of 1300°C is recommended to operate reliably the solar biomass gasifier with the considered biomass particle size range (0.3-4 mm) in a continuous feeding mode with complete biomass conversion, as verified by the carbon consumption rate that matches closely the carbon feeding rate. By optimizing biomass feeding rate consistently with operating temperature, the calorific value of the biomass feedstock is solar upgraded by 24% with carbon conversion extent above 90% and solar-to-fuel energy conversion efficiency up to 29%.

INTRODUCTION

Biomass and solar energy are promising sustainable renewable energy resources. Both of them can be well integrated via solar-driven gasification of biomass to convert solar energy and biomass into synthesis gas (syngas) [1,2]. The ideal stoichiometric steam-based gasification reaction of solid carbonaceous feedstock to syngas is written as:



Biomass feeding rate plays a significant role on the performance of the solar-driven biomass gasification process when dealing with a continuously fed solar reactor [3–5]. Increasing the biomass feeding rate is profitable for increasing syngas production capacity; however, excessively high biomass feeding rate may cause the incomplete biomass gasification, which in turn results in lower quality syngas and downgraded reactor performance, and possibly leads to the solid reactant accumulation inside the reactor cavity. The optimum mass flow rate of continuously-fed reactants needs to be determined for appropriate reactor operation. Indeed, for a given solar power input absorbed by the reactor, it can be anticipated that low feedstock flow rates will result in complete conversion but limited syngas production, whereas excessive flow rates result in solid reactant accumulation and temperature decrease because of

insufficient energy input. In both cases, the thermochemical reactor efficiency should not be optimal and therefore proper operating conditions need to be identified for maximizing the solar-to-chemical energy conversion efficiency, as the ultimate objective. The reactant feeding rate must closely match the rate of the gasification reaction. A trade-off thus exists between maximum allowable amount of injected feedstock and maximum chemical conversion to syngas. This trade-off can be addressed by optimizing the solar thermochemical efficiency of the reactor. Hence, optimization of the reactor performance by experimentally investigating the influence of biomass feeding rate with various carbonaceous feedstocks needs to be demonstrated.

In the present work, the aim was to experimentally investigate the effect of main process parameters including biomass feeding rate on syngas production yield, biomass gasification rate, and reactor performance in a 1.5 kW_{th} continuous particle-fed solar-irradiated gasifier designed on the basis of a spouted bed concept, which displays both enhanced heat and mass transfer and high solid residence time [4]. On-sun experiments were carried out with various biomass feedstocks at different biomass feeding rates up to 2.7 g/min at temperatures of 1100, 1200, and 1300 °C in order to identify the optimum biomass feeding rate with respect to maximum syngas production, composition (quality), and reactor performance at the considered temperatures, and insights into the process parameters effect on biomass gasification rate are also emphasized.

EXPERIMENTAL SETUP AND METHODS#

Fig.1 shows the operating principle of the steam gasification of biomass in the prototype continuous solar gasifier driven by highly concentrated sunlight, delivered by a 2 m-diameter parabolic concentrator located above the reactor, with a solar concentration ratio up to 10,551 suns (0.85 m focal distance, peak flux density of ~10.5 MW/m² for a Direct Normal Irradiation DNI of 1 kW/m²). More details on this solar reactor concept and design have been reported previously [3]. Three pressure sensors are employed to measure the pressure in the window area (P₁), reactor cavity (P₂), and hopper (P₃), and three temperature measurements (B-type thermocouples) are installed inside the cavity (T₁ and T₃) and external cavity wall surface (T₂). A solar-blind pyrometer placed at the center of the facedown parabolic concentrator also measures the temperature inside the cavity receiver to compare with T₁ and T₃.

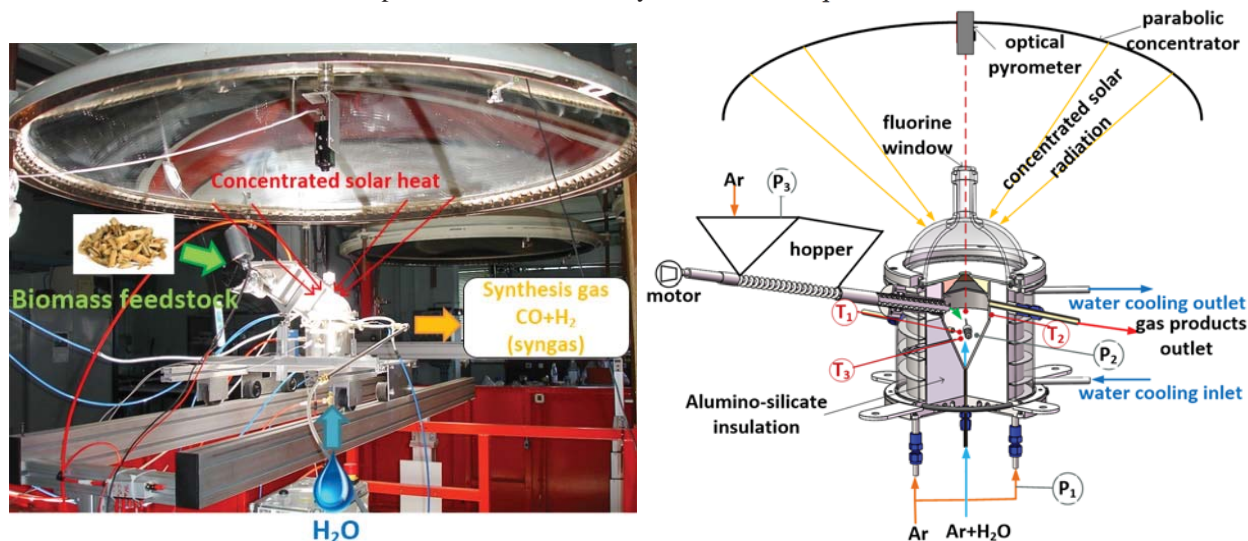


FIGURE 1. Photograph (left) and schematic illustration (right) of the steam gasification of biomass in a 1.5 kW_{th} prototype continuous solar reactor driven by real high-flux solar radiation

Five types of biomass feedstocks with different particle sizes (0.3-4 mm, Table 1) were prepared. Biomass feedstock (30 g) was subsequently loaded into the hopper, and the particle delivery system was then placed into the reactor injection port (Fig.1). The reactor was solar-heated to the desired temperature ranging from 1100 to 1300 °C. During reactor heating, Ar protective gas flows were supplied for protecting the window (2 Nl/min) and preventing the back-flow of hot gases through the screw path (0.5 Nl/min). Once the targeted temperature was stabilized, the steam was first supplied to the cavity receiver along with Ar carrier gas (0.2 Nl/min), and biomass was subsequently fed into the cavity in a continuous mode. Note that water was vaporized by the solar heat before entering the cavity

and was then entrained by the Ar flow at the tip of the cone, thus providing continuous steam flow inside the reactor. The steam/biomass ratio was kept constant at a slightly over-stoichiometric ratio (10% of excess water) by referring to Fig. 2 for any biomass feeding rates. This ratio was chosen to achieve complete gasification of the biomass whereas larger excess water would rather favor the water-gas shift reaction, according to previous experimental study [6]. The stoichiometric ratio ((x-z) in Eq. 1) depends on the type of biomass (chemical composition given in Table 1), and the theoretical H₂O/biomass stoichiometric molar ratio is two for biomass types A, B, and C and three for biomass types D and E, according to Eq. (1).

TABLE 1 Characteristics, ultimate and proximate analyses of the different feedstocks used for the experiments

Type	Biomass specie	Low heating value (MJ/kg)	Mean particle size (mm)	Apparent density (g/cm ³)	Proximate analysis (wt %)			Ultimate analysis (wt %)			
					Moisture	Ash	C	H	O	S	N
Type A	Beech (C ₆ H ₉ O ₄)	18.29	1	0.201	8.9	0.46	48.3	6.7	44.4	<0.1	0.11
Type B	Beech (C ₆ H ₉ O ₄)	18.38	4	0.222	8.9	0.57	48.5	6.7	44.1	<0.1	0.11
Type C	Resinous mix (C ₆ H ₁₁ O ₄)	17.66	0.55	0.194	7.3	0.46	49.9	7.1	42.4	<0.1	0.12
Type D	Resinous mix (C ₇ H ₁₁ O ₄)	18.3	0.3	0.140	9.3	0.29	52.8	7.1	40.7	<0.1	0.14
Type E	Resinous mix (C ₇ H ₁₁ O ₄)	17.4	2	0.124	9.2	0.28	52.3	7.2	40.1	<0.1	0.09

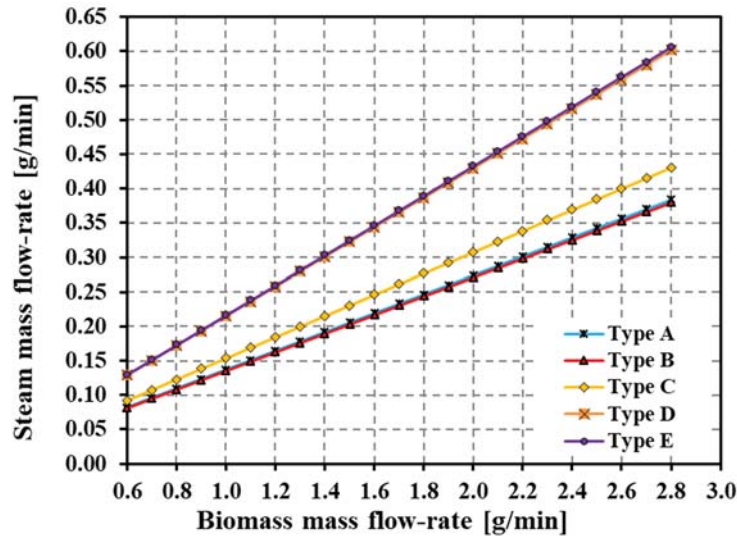


FIGURE 2. Relation between the mass flow rates of steam and biomass feedstocks for a stoichiometric steam/biomass ratio (accounting for the moisture content in the feedstock)

The produced syngas exits the reactor outlet and continuously flows through a gas washing unit (scrubber) comprising a bubbler and two micro-filters to remove unconverted water and entrained char particles, respectively. Product gas species (H₂, CO, CO₂, CH₄) are then analyzed by an on-line syngas analyzer; meanwhile, a small stream of product gases is diverted to a gas chromatograph (GC) for chemical analysis every 2 min. The GC is also used to quantify the amount of secondary non-condensable hydrocarbons, including mainly C₂H₂ and C₂H₄ (total amount noted as C₂H_m). The syngas yields (mmole per gram dry biomass, mmol/g_{biomass}) are calculated by time integration of the syngas production rates over the experiment duration. The solar-to-fuel energy conversion efficiency, energy upgrade factor, carbon conversion, and thermochemical reactor efficiency are calculated to report the reactor performance during continuous solar steam gasification of biomass.

The solar-to-fuel energy conversion efficiency ($\eta_{solar-to-fuel}$) is defined as the ratio of the chemical energy of the syngas produced to the total energy input, which is the summation of the solar power input and the lower heating value of the feedstock:

$$\eta_{solar-to-fuel} = \frac{(LHV_{syngas} \cdot \dot{m}_{syngas})}{\dot{Q}_{solar} + (LHV_{feedstock} \cdot \dot{m}_{feedstock})} \quad (2)$$

Where LHV_{syngas} and $LHV_{feedstock}$ are the lower heating values (J/kg), \dot{m}_{syngas} and $\dot{m}_{feedstock}$ are the mass flow rates (kg/s) of syngas products and biomass feedstock, respectively, and \dot{Q}_{solar} is the solar power input (W).

The energy upgrade factor (U) is calculated by the ratio of the energy content of the chemical products to that of the processed biomass feedstock:

$$U = \frac{LHV_{syngas} \cdot \dot{m}_{syngas}}{LHV_{feedstock} \cdot \dot{m}_{feedstock}} \quad (3)$$

The carbon conversion (X_C) is defined as the ratio of the carbon yield in the syngas to the initial amount of carbon in the biomass feedstock (F_i represents the molar flow rate of species i, mol/s):

$$X_C = \frac{\int_0^t F_{CO}(t)dt + \int_0^t F_{CO_2}(t)dt + \int_0^t F_{CH_4}(t)dt + \int_0^t 2F_{C_2H_m}(t)dt}{\int_0^t x F_{C_xH_yO_z}(t)dt} \quad (4)$$

The thermochemical reactor efficiency represents the ratio of solar energy absorbed by the reactor that is used for driving the chemical reaction (reaction enthalpy) and for heating the steam, inert gas and solid reactant:

$$\eta_{reactor} = \frac{\dot{Q}_{heating} + \dot{Q}_{reaction}}{\dot{Q}_{solar}} \quad (5)$$

For this study, 49 on-sun runs have been successfully performed to gain insights into process parameters influence (biomass feeding rate, temperatures) on performance outputs.

RESULTS AND DISCUSSION

Syngas Production Yield

H₂, CO, CO₂, CH₄ and C₂H_m yields as a function of biomass feeding rate ($\dot{m}_{feedstock}$) for biomass type A, B, C, D, and E at 1100, 1200, and 1300 °C are shown separately in Fig. 3. Syngas yields were determined in the $\dot{m}_{feedstock}$ ranges of 0.8-1.5 g/min at 1100 °C, 0.6-2.2 g/min at 1200 °C, and 0.8-2.7 g/min at 1300 °C. At 1100 °C, the lowest H₂ and CO yields and the highest CO₂, CH₄, and C₂H_m yields were observed, resulting from low gasification kinetics evidenced by the presence of pyrolytic gases in previous study [7]. As a result, the maximum $\dot{m}_{feedstock}$ can only reach 1.5 g/min, and no optimal $\dot{m}_{feedstock}$ could be identified at this temperature. At 1200 °C, $\dot{m}_{feedstock}$ was increased up to 2.2 g/min, and all gas yields rose with increasing $\dot{m}_{feedstock}$. When compared to 1100 °C, H₂ (Fig. 3a) and CO (Fig. 3b) yields at 1200 °C were higher while CO₂, CH₄ and C₂H_m yields were lower as a result of the improved kinetics of gasification, e.g. char gasification (C+H₂O→CO+H₂) and methane reforming (CH₄+H₂O→CO+3H₂). At this temperature, the $\dot{m}_{feedstock}$ of biomass type C reached its optimal point at 2.2 g/min (reflected by a stable pattern in H₂, a slight decrease in CO, and a significant increase in CO₂, CH₄, and C₂H_m). At 1300 °C, the highest H₂ and CO yields and the lowest CO₂, CH₄, and C₂H_m yields were noticed, demonstrating the highest syngas quality as well as syngas yield at this temperature. Moreover, the optimal $\dot{m}_{feedstock}$ of biomass type A was approached, as evidenced by stable H₂ and CO yields at 2.5-2.7 g/min, while that of biomass type C and biomass type D were determined to be 2.5 and 1.8 g/min, respectively. For example, the H₂ and CO yields for biomass type C reached the maximum value of 39.2 and 29.1 mmol/g_{biomass} at 2.5 g/min and then reduced to 37.6 and 27.9 mmol/g_{biomass}, respectively, at 2.7 g/min, while the amounts of CO₂, CH₄, and C₂H_m for biomass type C reached the maximum value of 4.0, 3.2, and 1.4 mmol/g_{biomass}, respectively, at 2.7 g/min, thus confirming the optimal feeding rate at 2.5 g/min. However, the optimum feeding point could not be found for the other biomass types due to the limitation of the maximum feeding rate. Trends of H₂ yield between biomass types A and B and between biomass types D and E for any temperatures were not significantly different as a result of their similar initial chemical composition (Table 1). The H₂ yields for biomass types D and E were considerably higher than for the other types owing to their higher initial hydrogen content (Table 1) while the trends of CO for each biomass were similar. In addition, smaller particle size showed a positive effect on syngas yield resulting from enhanced heat and mass transfer rates [8–10]. However, their compared trends (type A vs. type B, and

type D vs. type E) remained similar. Hence, the biomass type (composition) showed more significant influence on syngas yield than the biomass particle size in the considered size range (0.3-4 mm). In summary, increasing the $\dot{m}_{\text{feedstock}}$ enhanced syngas yield, at the expense of an increase in CO_2 , CH_4 , and C_2H_m yields due to a lowered gas residence time, thereby showing adverse impact on syngas quality. This issue can be tackled by increasing the temperature to enhance the reaction kinetics, which in turn increases biomass consumption and syngas quality. However, exceeding an optimal $\dot{m}_{\text{feedstock}}$ point led to a reduction in syngas yield and biomass accumulation, as evidenced by biomass type C at 2.7 g/min. The optimal biomass feeding rate was 2.2 g/min (1200 °C) and 2.5 g/min (1300 °C) for biomass type C, 1.8 g/min (1300 °C) for biomass type D, and was approached at 2.7 g/min for biomass type A. It could not be determined at 1100 °C because of pyrolytic gases generating smoke issue caused by low reaction kinetics as mentioned before.

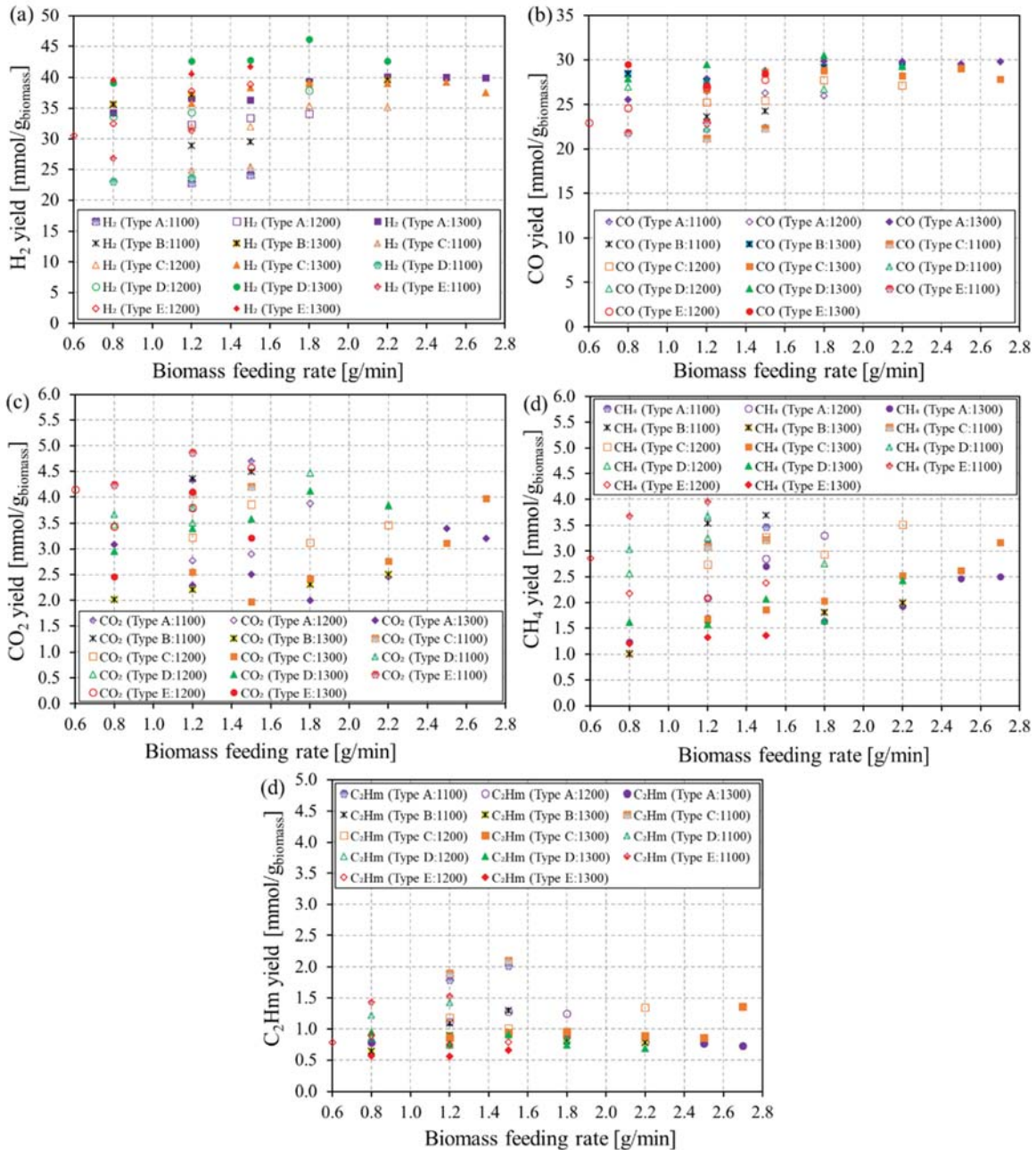


FIGURE 3. Syngas yields for different biomass feedstocks as a function of biomass feeding rate at 1100 °C, 1200 °C, and 1300 °C.

Biomass Gasification Rate

The biomass gasification rate (equivalent to the carbon consumption rate) was determined as a function of the carbon feeding rate at 1100, 1200, and 1300 °C for biomass types A, B, C, D, and E, and was further compared to the ideal carbon consumption rate for each biomass type (equal to the carbon feeding rate, i.e. the carbon contained in the fed biomass), as presented in Fig. 4. The carbon consumption rate is quantified by the summation of the nominal production rates of CO, CO₂, and CH₄ contained in the produced syngas (assuming that the C consumption rate and the summation of production rates of carbon-containing gas species are equivalent), and achieved during continuous biomass injection (at steady state). The carbon consumption rate increased when increasing both temperature and biomass feeding rate regardless of biomass type. Typically, at 1300 °C the carbon consumption rate closely matched the carbon feeding rate at low feeding rates (linear tendency at 0.4-0.7 g/min), which also means that the reactant feeding rate closely matched the rate of the gasification reaction. From a threshold value of carbon feeding rate, the carbon consumption rate became slightly lower than the carbon feeding rate at above 0.8 g/min (1300 °C), which means that the gasification rate was not high enough to convert totally the injected biomass. In other words, from this point, carbon accumulation in the reactor (due to incomplete biomass gasification) may occur if the feeding rate is too high with respect to the reactor capacity. An optimal value was observed for biomass type C at a carbon feeding rate of ~1.16 g/min (corresponding to 2.5 g/min of biomass feeding rate at 1300 °C). Both the carbon consumption rates and carbon feeding ranges at 1300 °C were greater and closer to the ideal carbon consumption rates for any biomass types, compared to those obtained at 1200 °C and 1100 °C. This is because the higher gasification kinetics at 1300 °C resulted in both higher carbon consumption rate and carbon feeding range. The impact of biomass feeding rate on syngas production capacity and reactor performance was thus evidenced. The carbon consumption rate at 1300 °C matched closely the carbon feeding rate (provided the feeding rate was below a threshold value regardless of the biomass type). This means that 1300 °C is a suitable temperature to operate reliably the solar biomass gasifier in a stable continuous mode with a biomass conversion rate equal to the feeding rate.

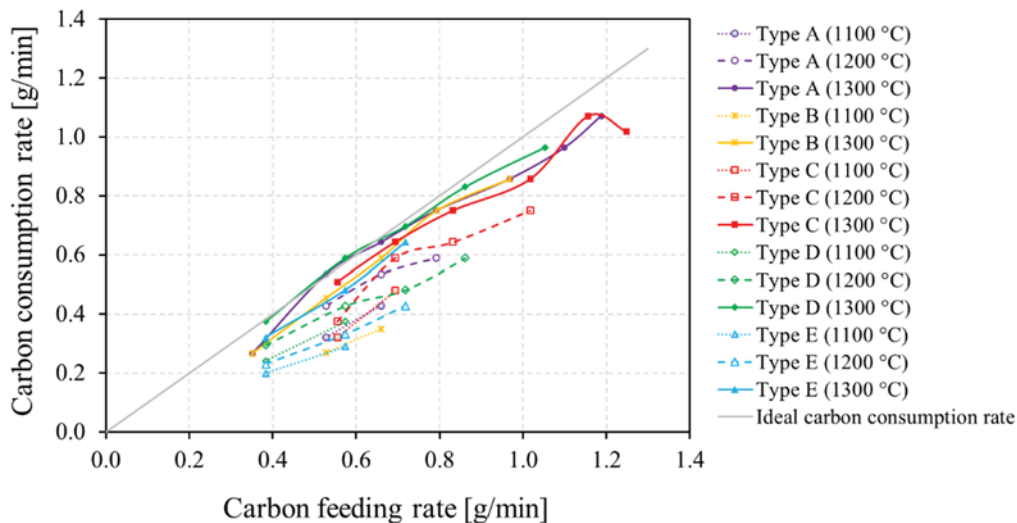


FIGURE 4. Comparison of the effect of carbon feeding rate on carbon consumption rate for each biomass type at 1100, 1200, and 1300 °C

Reactor Performance and Efficiencies

The solar reactor performance at 1000 °C, 1200 °C, and 1300 °C for the representative biomass types A, C, and D have been compared, according to Fig. 5. Note that the results of biomass types B and E were omitted as they are similar to the ones of biomass types A and D, respectively, due to similar chemical biomass composition. As expected, both U (Fig. 5a) and X_C (Fig. 5b) increased with $\dot{m}_{\text{feedstock}}$ regardless of temperature and biomass type. At 1300 °C, trends in U and X_C clearly leveled off at above 1.8 g/min, pointing out the optimal biomass feeding rate, and the maximum U values of 1.14, 1.10, 1.16, 1.20 and 1.15 (1.19, 1.15, 1.22, 1.24 and 1.19 when accounting for C₂H_m)

were identified for biomass types A (at 2.7 g/min), B (at 2.2 g/min), C (at 2.5 g/min), D (at 1.8 g/min) and E (at 1.5 g/min), respectively. The optimal $\dot{m}_{feedstock}$ with respect to the highest U value at 1300 °C was found at 2.5 and 1.8 g/min for biomass types C and D, respectively. These types of biomass exhibit the lowest particle sizes; hence, their gasification rate is more sensitive to the feeding rate. The overlapped trends of U between biomass types A and B and between biomass types D and E were due to their similar chemical properties, indicating a negligible impact of the biomass particle size on U for the considered size range (0.3–4 mm). In addition, the evolution of U consistently followed the same trend as X_C (Fig. 5b). The highest and lowest X_C values of 88.6% and 72.9% (90.4% and 76.2% when accounting for C_2H_m) were obtained for biomass type A at 1300 °C (2.7 g/min) and biomass type E at 1100 °C (0.8 g/min), respectively. In comparison, both U and X_C values at 1300 °C were higher than those obtained at 1200 and 1100 °C (U and X_C in the range of 1.04-1.10 and 80.4-84.2% at 1300 °C compared to 0.91-0.95 and 77.6-79.8% at 1100 °C for biomass type A), thus confirming the enhancement of syngas yield and reaction extent at 1300 °C. Moreover, a rise in $\dot{m}_{feedstock}$ increased $\eta_{solar-to-fuel}$ (Fig. 5c) because the total solar energy input (Fig. 5d) was lowered (due to the significant reduction in the biomass injection duration) even though the solar power input (Fig. 5f) was increased consistently with $\dot{m}_{feedstock}$ for maintaining the isothermal operating temperature. For example, $\eta_{solar-to-fuel}$ for biomass type A increased from 12.4% at 0.8 g/min to 26.6% at 2.7 g/min. The maximum $\eta_{solar-to-fuel}$ values of 26.6%, 25%, 27.6%, 25.3%, and 21.2% (27.8%, 26.0%, 29.0%, 26.3%, and 21.8% when accounting for C_2H_m) were achieved for biomass types A (at 2.7 g/min), B (at 2.2 g/min), C (at 2.5 g/min), D (at 2.2 g/min) and E (at 1.5 g/min), respectively. The $\eta_{solar-to-fuel}$ of biomass type C noticeably decreased at 2.7 g/min, confirming that exceeding the optimal $\dot{m}_{feedstock}$ feeding point adversely resulted in incomplete gasification, thus leading to solid reactant accumulation and temporal stop in the biomass feeding to let the accumulated reactant being gasified. In this case, the injection duration was in turn extended, leading to an increase in the solar energy input (Fig. 5d). In comparison, $\eta_{solar-to-fuel}$ (Fig. 5c) at 1200 °C was slightly higher than that at 1300 °C as both the solar energy (Fig. 5d) and power inputs (Fig. 5f) were considerably lower, while the product syngas yield was not drastically different. For example, $\eta_{solar-to-fuel}$ for biomass type A was in the range of 18.1-20.6% at 1200 °C compared to 17.3-20.8% at 1300 °C, respectively. However, $\eta_{solar-to-fuel}$ at 1100 °C was still lower than that at 1200 °C as a result of the downgraded gasification performance. Similar to $\eta_{solar-to-fuel}$, $\eta_{reactor}$ (Fig. 5e) rose with $\dot{m}_{feedstock}$, ranging between 15.3-25.3%, 17.3-24.2%, 17.9-27.0%, 16.1-24.0% and 15.7-21.2% for biomass types A, B, C, D and E, respectively, indicating an efficient solar energy utilization and conversion, and leading to a reduction of the heat losses. Moreover, $\eta_{reactor}$ dropped when $\dot{m}_{feedstock}$ was over its optimum point (2.5 g/min for biomass type C) as a result of biomass accumulation and extension of the reaction duration, as mentioned before. In summary, an increase in both biomass feeding rate and temperature is substantially favorable for increasing solar gasification performance because reaction kinetics and biomass consumption rates are enhanced. However, heat losses increase consistently with temperature, which adversely leads to a reduction in both $\eta_{solar-to-fuel}$ and $\eta_{reactor}$ at 1300 °C. The maximum U, X_C , $\eta_{solar-to-fuel}$, and $\eta_{reactor}$ were consistently obtained at the optimal feeding point, in agreement with maximum syngas yield and biomass gasification rate (Fig. 3 and 4).

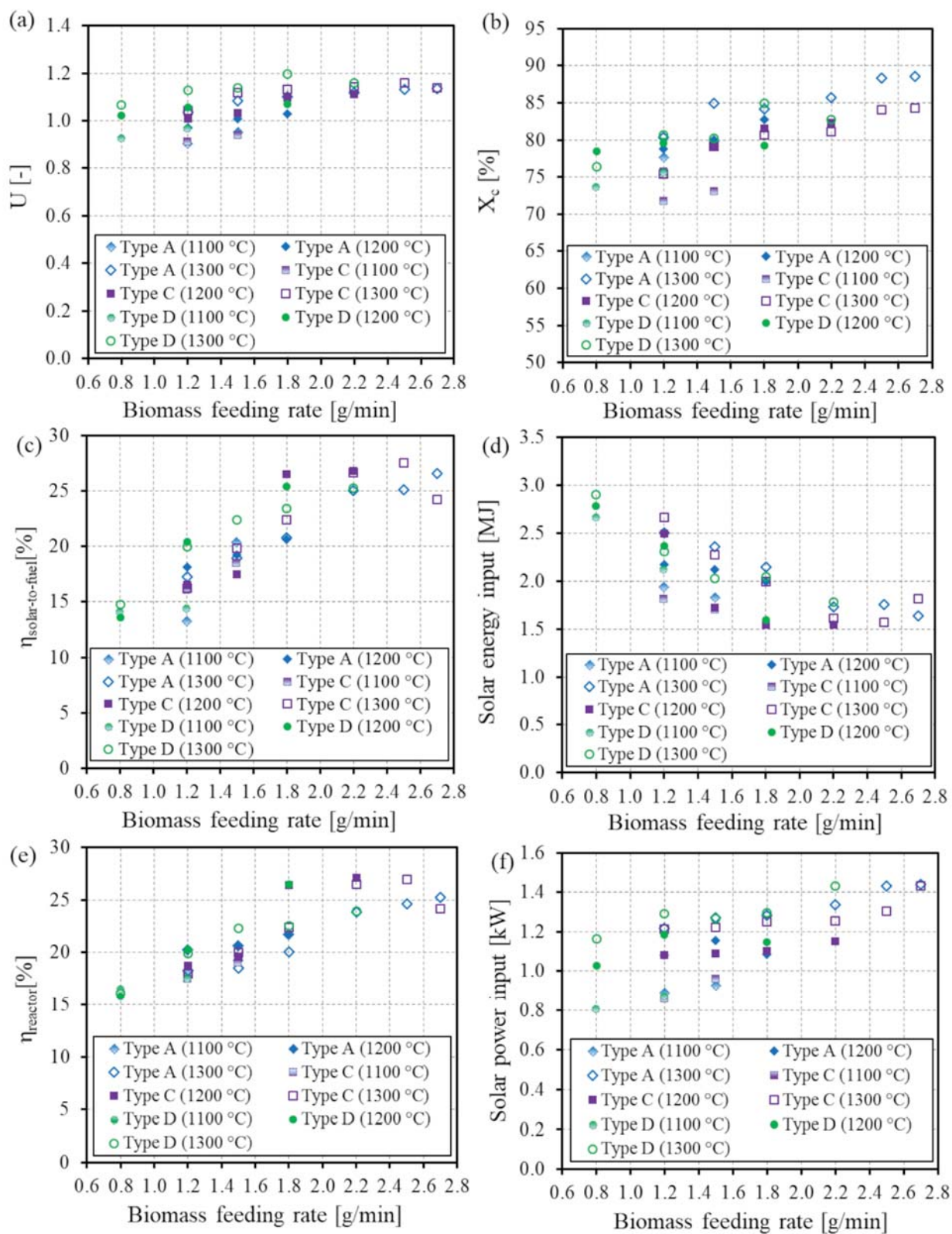


FIGURE 5. Comparison of the effect of biomass feeding rate at 1100 °C, 1200 °C and 1300 °C on (a) energy upgrade factor (b) carbon conversion, (c) solar-to-fuel energy conversion efficiency, (d) solar energy input, (e) thermochemical reactor efficiency and (f) solar power input (C_2H_m not included in the calculation)

CONCLUSION

A 1.5 kW_{th} particle-fed solar-irradiated gasifier has been tested for on-sun continuous steam gasification of biomass. The influence of biomass feeding rate on syngas yield, biomass gasification rate, and reactor performance has been experimentally evaluated with various lignocellulosic biomass feedstocks in the temperature range 1100–1300 °C, delivered by highly concentrated sunlight, thereby storing intermittent solar energy into syngas. An increase in biomass feeding rate significantly promoted syngas yield and reactor performance; however, exceeding the optimal biomass feeding point showed an adverse effect on produced syngas. Indeed, H₂ and CO yields decreased at the expense of a growth in C₂H_m, CH₄, and CO₂ due to a reduction of the gas residence time, and eventually biomass accumulation issues and pyrolytic gases emissions may occur. Increasing temperature (1100–1300 °C) significantly enhanced reaction extent, syngas quality (low C₂H_m, CH₄, and CO₂ yields), and reaction kinetics, which in turn increased biomass consumption rates matching biomass feeding rate. At 1300 °C, the biomass feeding rate reached its optimum point at up to 2.5 g/min for biomass type C (1.8 g/min for biomass type D), whereas at 1200 °C the optimal biomass feeding point was found at 2.2 g/min (biomass type C) corresponding to the nominal feeding rate for this 1.5 kW_{th} solar reactor. However, heat losses rose consistently with temperature, which adversely led to a reduction in both $\eta_{\text{solar-to-fuel}}$ and η_{reactor} at 1300 °C. The effect of biomass composition showed more significant influence on syngas production than biomass particle size (0.3–4 mm). Moreover, increasing temperature and biomass feeding rate enhanced biomass gasification rate (carbon consumption rate). At 1300 °C, the carbon consumption rates were greater than those obtained at 1200 and 1100 °C, and their values were closer to the ideal maximum carbon consumption rate for any biomass type. The energy upgrade factor, reaction extent (carbon conversion), solar-to-fuel energy conversion efficiency, and thermochemical reactor efficiency increased with biomass feeding rate because the total solar energy input during processing was decreased, resulting from a shortened biomass injection duration (maximum achieved values (accounting for C₂H_m) up to 1.24, 90.4%, 29.0%, and 27.0%, respectively). Optimizing the biomass feeding rate consistently with operating temperature is beneficial for continuous solar biomass gasification. It aims to enhance biomass consumption rate, reaction kinetics, as well as reaction extent (carbon conversion) for maximizing syngas yield and quality and minimizing heat losses. Apart from increasing the heat losses, the temperature of 1300 °C is recommended to operate reliably the solar biomass gasifier in a stable continuous mode with a biomass conversion rate matching well the feeding rate thanks to greater reaction kinetics, biomass consumption rate, reaction extent (carbon conversion), syngas yield, and syngas quality (because of lower CH₄, CO₂ and C₂H_m yields).

ACKNOWLEDGEMENTS

The authors would like to gratefully acknowledge the King Mongkut's Institute of Technology Ladkrabang (KMITL), Thailand and Campus France, Thailand for Ph.D. scholarship support.

REFERENCES

- 1 R.W. Taylor, R. Berjoan, J.P. Coutures, *Sol. Energy*. **30** (1983) 513–525.
- 2 S. Rodat, Q. Bellouard, S. Abanades, S. Chuayboon, P.-E. Frayssines, S. Ravel, *AIP Conf. Proc.* **2033** (2018) 130012.
- 3 S. Chuayboon, S. Abanades, S. Rodat, *Renew. Energy*. **130** (2019) 360–370.
- 4 Q. Bellouard, S. Abanades, S. Rodat, *Energy & Fuels*. **31** (2017) 10933–10945.
- 5 S. Chuayboon, S. Abanades, S. Rodat, H. Boujjat, *AIP Conf. Proc.* **2126** (2019) 180006.
- 6 S. Chuayboon, S. Abanades, S. Rodat, *Chem. Eng. Process. Process Intensif.* **125** (2018) 253–265.
- 7 S. Chuayboon, S. Abanades, S. Rodat, *Fuel Process. Technol.* **182** (2018) 1–14.
- 8 A. Z'Graggen, P. Haueter, D. Trommer, M. Romero, J.C. de Jesus, A. Steinfeld, *Int. J. Hydrogen Energy*. **31** (2006) 797–811.
- 9 P. Holmgren, D.R. Wagner, A. Strandberg, R. Molinder, H. Wiinikka, K. Umeki, M. Broström, *Fuel*. **206** (2017) 342–351.
- 10 A. Trubetskaya, G. Beckmann, J. Wadenbäck, J.K. Holm, S.P. Velaga, R. Weber, *Fuel*. **206** (2017) 675–683.